Available online at website: https://journal.bcrec.id/index.php/bcrec

Bulletin of Chemical Reaction Engineering & Catalysis, 21 (2) 2026, 452-466

Original Research Article

Comparative Evaluation of Fe-MOF, Cu-MOF, and Bimetallic Fe/Cu-MOF for Enhanced CO_2 Adsorption: Synthesis, Characterization, and Performance Analysis

Nor Khonisah binti Daud*, Hamidah binti Abdullah, Nur Aminatulmimi binti Ismail

Faculty of Chemical & Process Engineering Technology, Universiti Malaysia Pahang Al-Sultan Abdullah, Lebuh Persiaran Tun Khalil Yaakob, 26300 Kuantan, Malaysia.

Received: 28th January 2026; Revised: 25th February 2026; Accepted: 26th February 2026
Available online: 28th February 2026; Published regularly: August 2026

Abstract

Rising atmospheric CO_2 concentrations necessitate the development of efficient and economically viable carbon capture materials. Metal-organic frameworks (MOFs) offer strong potential due to their tunable pore structures and accessible metal sites. In this work, Fe-MOF, Cu-MOF, and bimetallic Fe/Cu-MOF were synthesized via a solvothermal route and systematically evaluated for CO_2 adsorption performance. The materials were characterized using SEM-EDX, FTIR, XRD, BET, and TGA to establish correlations between structural properties and adsorption behavior. CO_2 uptake was investigated under varying pressure (1-5 bar), adsorbent dosage (0.2-0.5 g), and temperature (40-50 °C). Among the three adsorbents, Fe/Cu-MOF exhibited the highest adsorption capacity, reaching 3.22 $mg.g^{-1}$ at 5 bar, outperforming Fe-MOF (2.54 $mg.g^{-1}$) and Cu-MOF (2.35 $mg.g^{-1}$). Adsorption increased markedly with pressure, showed non-linear dependence on dosage due to site underutilization and diffusion limitations, and decreased with increasing temperature, indicating an exothermic physisorption-dominated process. BET analysis revealed that Fe/Cu-MOF possessed the highest surface area (19.4 $m^2.g^{-1}$) and pore volume (0.0489 $cm^3.g^{-1}$), while XRD and FTIR confirmed successful incorporation of both metal centers, generating chemically heterogeneous adsorption sites. Kinetic analysis demonstrated that CO_2 uptake follows a pseudo-first-order model, consistent with surface-controlled physisorption. The enhanced performance of Fe/Cu-MOF is attributed to synergistic effects arising from dual-metal coordination, improved pore connectivity, and increased availability of active adsorption domains. These findings highlight the potential of bimetallic Fe/Cu-MOFs as promising candidates for pressurized CO_2 capture applications and provide insight into structure-performance relationships governing gas adsorption in defect-rich MOF systems.

Keywords: Carbon Capture Materials; CO_2 adsorption; Metal-Organic Frameworks adsorbents; Solvothermal Route

How to Cite: Daud, N. K., Abdullah, H., Ismail, N. A. (2026). Comparative Evaluation of Fe-MOF, Cu-MOF, and Bimetallic Fe/Cu-MOF for Enhanced CO_2 Adsorption: Synthesis, Characterization, and Performance Analysis. *Bulletin of Chemical Reaction Engineering & Catalysis*, 21 (2), 452-466. (DOI: 10.9767/bcrec.20658)

Permalink/DOI: https://doi.org/10.9767/bcrec.20658

1. Introduction

Increasing atmospheric CO_2 concentrations have evolved into among the most urgent environmental issues of our day because CO_2 emissions worldwide are rising to previously unheard-of levels and greatly impact climate change. This condition has ignited thorough investigation on several approaches for carbon capture, with a particular underscoring on the development of reasonably priced and effective adsorbent materials [1-2]. Metal-organic frameworks (MOFs) are attractive alternatives for conventional materials due to the large surface area, incomparable porosity, and capacity for chemical modification. MOFs are particularly best suited for application concerning the selective adsorption and separation of gases due to these characteristics [3-6].

The fact that copper metal centres, which provide efficient binding sites for CO_2 molecules

* Corresponding Author.
Email: khonisah@umpsa.edu.my (N. K. Daud)

by certain metal-CO_2 interactions, has raised significant interest in copper-based metal-organic frameworks (Cu-MOFs). Furthermore, the framework's stability as well as its CO_2 selectivity can be upgraded by carefully designing the Cu-MOFs' organic linkers. Considering the richness of copper, as well as its well-defined coordination chemistry, Cu-MOFs are of significant interest from an economic as well as practical consideration [7-9].

Iron-based metal-organic frameworks (Fe-MOFs), particularly MIL-101(Fe) and MIL-53(Fe), are highly effective for CO_2 adsorption due to their high surface area, large pore volume, and stability. These materials are considered strong candidates for industrial carbon capture from flue gases, as they exhibit excellent stability in the presence of water and high thermal resistance [10-12].

Iron- (Fe) and copper- (Cu) based metal-organic frameworks (MOFs) systems have emerged as preeminent candidates for gas storage and capture, offering substantial potential due to their high porosity, tunable pore structures, and exceptional surface areas. Their ability to be modified with open metal sites (OMSs) and tailored organic ligands allows them to excel in capturing specific gases, including CO_2, CH_4 and H_2, often outperforming traditional porous materials like zeolites. Nevertheless, each has its shortcomings. While possessing good adsorption capacities, Cu-MOFs typically have the issue of instability and low selectivity. However, even as their copper-based counterparts did not surpass performance in adsorption due to the higher costs and instability of the former, Fe-MOFs did the same [13-14]. Among the key shortcomings preventing the creation of better reliable and effective gas capture systems is overcoming such limitations. Focusing on Cu/Fe-MOFs design and synthesis, the work endeavors on the discovery of new methods of adsorbing the CO_2 through novel methods. While through the hybridization of the benefits of the individual iron and copper MOFs, the work looks at tuning such materials through a hybrid approach. This one tries to overcome the shortcomings of each material through hybridizing the benefits of each type to promote their selectivity, stability, as well as adsorption capacities.

By enhancing the viability and efficiency of application of such materials in industries, the present work aims to cut the impact of the release of greenhouse gases on global warming by a considerable level. Due to their characteristic bimetallic nature, increased porosity, and adjustable adsorption sites, Fe/Cu-MOFs have proven to be extremely effective adsorbents from the available literature [15]. The synergistic impact of the presence of iron and copper in the adsorption mechanism of the MOF greatly surpasses the adsorption efficiency of single-metal MOFs and provides a possible route for the enhanced sequestration of CO_2 [16].

Adsorption of organic dyes, heavy metals, and emerging pollutants is enhanced by the intermediate crystallinity and large surface area of Fe/Cu-MOFs. It has been shown through studies that Fe/Cu-MOFs can effectively remove dyes such as methylene blue and Congo red through electrostatic forces, π-π stacking, and coordination bonding with metal sites [15]. Besides, due to the strong coordination of metal sites and MOF function groups and the presence of redox-active Fe sites to assist in the sequestration of the heavy metals, the adsorption capacity of Fe/Cu-MOFs have been extensively examined for the adsorption of the heavy metals. From the studies, the MOFs have excellent affinities toward Pb^{2+}, Cd^{2+}, and Cr^{6+} [17]. The adsorption capacity of Fe/Cu-MOFs to catalyze the degradation of pollutants in advanced oxidation processes has also been examined. The iron sites of the frameworks enhance the generation of reactive oxygen species (ROS), which enhance the degradation of the pollutants through the generation of hydrogen peroxide (H_2O_2) or peroxymonosulfate (PMS) [18]. These findings exhibit the application prospects of Fe/Cu-MOFs as adsorbents with extensive application prospects in the field of environmental remediation. The extensive application instances of the adsorbents in the industrial system for the adsorption of CO_2 remain drastically inhibited by considerations such as the decrease in the costs of production as well as the prospects of scale-up as well as long-term stability of the structures, despite these developments. Additional study should be performed to enhance sustainable approaches to carbon capture to fully realize the application prospects of the adsorbents toward practical applications and assist in the reduction of the emissions of greenhouse gases.

This work investigated the impact of adsorbent dose, operating pressure, and temperature on adsorption effectiveness as well as kinetic study with a view to analyzing the adsorption performance of Fe-MOF, Cu-MOF, and bimetallic Fe/Cu-MOF for CO_2.

2. Materials and Method

2.1. Materials and Chemicals

$CuSO_4 \cdot 5H_2O$, $Fe(NO_3)_3 \cdot 9H_2O$, ethanol, isopropanol, trimesic acid, and N, N-dimethylformamide (DMF) were the components used to create the adsorbents. Capital Eng. Resource Sdn. Bhd. provided all the reagents.

2.2. Synthesis of MOFs

The MOFs utilized in this study were synthesized using the solvothermal method [9]. To prepare Fe-MOF, $Fe(NO_3)_3 \cdot 9H_2O$ (5.90 g; 0.0146 mol) and trimesic acid (3.07 g; 0.0146 mol) were combined and transferred into a 250 mL round-bottom Schott glass flask. A solution consisting of N, N-dimethylformamide (DMF) and isopropanol with a volumetric ratio of 20:1 which contained 12.5 mL of DMF and 237.5 ml of isopropanol was mixed to the same Schott glass. At room temperature, the blend was agitated until every solid had been totally dissolved. An oven preheated to 80 °C is used to hold a uniform reaction mixture for eighteen hours. After cooling to ambient temperature, the product was filtered and rinsed three times with methanol to remove any last impurities. The finished product was then produced by drying the material for 12 hours at 120 °C in a vacuum oven. The manufacturing of Cu-MOF and Cu/Fe-MOF were done using the same methods.

2.3. Characterization Techniques

A Leo Supra VP Field Emission Scanning Electron Microscope (FE-SEM) working at 20 kV with a 3.0 beam size under high-vacuum circumstances and a ZEISS Merlin High-Resolution SEM operating within a voltage range of 5-20 kV were applied to analyze the surface morphology of the produced products. Using the Oxford INCA 400 system, energy dispersive X-ray spectroscopy (EDX) was employed to study the composition of elements. Fourier Transform Infrared (FTIR) spectroscopy was performed using a Perkin Elmer FTIR-2000 to identify surface functional groups using a 1:10 mg ratio of KBr to adsorbent. Spectra were captured between 4000 and 500 cm^{-1}. A thermogravimetric analyzer (TGA), model SDTGA1200, was used to measure thermal stability between 25 and 900 degrees Celsius in a nitrogen atmosphere at a steady 5 degrees Celsius per minute heating rate. An X-ray diffractometer (XRDynamic 500) was used to study crystalline phases, scanning over a 2-theta range of 5° to 60°. Using a Micromeritics ASAP 2020 device, nitrogen adsorption at 77 K was used to calculate the Brunauer-Emmett-Teller (BET) surface area.

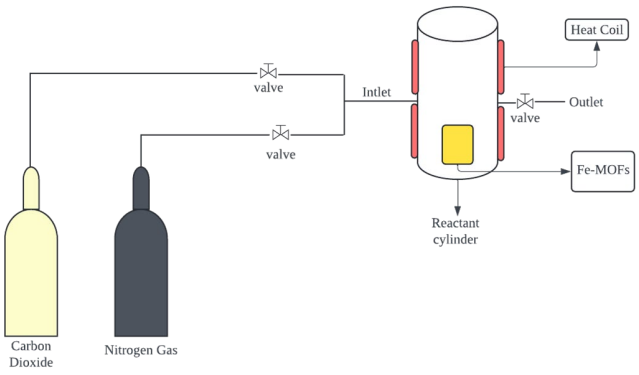

Figure 1. CO_2 adsorption experimental rig.

2.4. CO_2 Adsorption Study

CO_2 adsorption experiments were conducted employing a custom-designed setup, featuring a metallic tubular container that served as the reactor, as illustrated in Figure 1. A control panel was attached to the reactor to track the process's operational temperature and pressure. To determine the baseline concentration of pure CO_2, preliminary tests were conducted without the use of any adsorbent. The reactor was then filled with a predetermined volume of adsorbent, and the system was adjusted to the required pressure and temperature. CO_2 was then introduced into the reactor, initiating the adsorption process once the target parameters were reached. The concentration of the exiting gas was measured using a Lutron CO2-9914SD CO_2 meter.

The measurement of CO_2 adsorption expressed through q_t ($mg.g^{-1}$) remains essential when evaluating how effective MOF materials perform in CO_2 capture. Equations (1) and (2) were used to calculate the CO_2 adsorption along with the reactor's volume V (L), the adsorbent's mass m (g), the initial CO_2 concentration C_0, the CO_2 concentration at interval time, C_t (ppm), the operating pressure (Pa), the ambient temperature (K), the universal gas constant, R (8.314 $J \cdot mol^{-1} \cdot K^{-1}$) and the molecular weight of CO_2, M_{CO2} (44 $g.mol^{-1}$).

$$n = \frac{(C_0 - Ct)}{10^6} \cdot \frac{PV}{RT} \quad (1)$$

$$q_t = \frac{n \cdot M_{CO_2}}{m_{ads}} \quad (2)$$

2.4.1 Effect of dosage

The amount of adsorbent was varied (0.2, 0.3 and 0.4 g) to determine its influence on adsorption capacity with the other parameters were kept constant (P = 1 bar, T = 30 °C and volumetric flowrate ratio of CO_2:N_2=15:85). A fixed volume of gases (CO_2 and N_2) was introduced into the adsorption chamber, and the mass of the adsorbent was incrementally increased. The relationship between adsorbent dosage and adsorption efficiency was analyzed to identify the optimal adsorbent amount for maximum gas uptake.

2.4.2 Effect of pressure

By altering the gas pressure inside the adsorption chamber, the impact of pressure on adsorption capacity was investigated. Adsorption tests were conducted at different pressures (1, 2, 3, 4 and 5 bar) to evaluate how pressure influences the ability of the adsorbents to capture CO_2.

2.4.3 Effect of temperature

The effect of temperature changes on adsorption performance was examined. Adsorption tests were carried out at different temperatures (40, 45, and 50 °C) to assess the MOFs' adsorption capacity.

2.5. CO_2 Adsorption Kinetic Models

The CO_2 adsorption kinetics of mono- and bimetal-based MOFs adsorbents were examined in this work using three different kinetic models: Avrami's fractional-order models, Pseudo-First Order (PFO), and Pseudo-Second Order (PSO).

2.5.1 Pseudo-First Order (PFO) model

PFOs are typically used to predict how physical adsorbents will behave when adsorbed [19,20]. It was first suggested in 1898 by Lagergren [21] on the grounds that the quantity of available adsorption sites determines the rate of adsorption. The whole adsorption process is thought to be under control during the diffusion step. The PFO model can be expressed using the equation that follows:

$$Log\ (Q_e - Q_t) = log\ Q_e - k_1 t \quad (3)$$

where k_1, Q_t, and Q_e are the adsorption rate constant, the amount of CO_2 sorbed at any time ($mg.g^{-1}$) and at the equilibrium ($mg.g^{-1}$), respectively.

2.5.2 Pseudo-Second Order (PSO) model

The PFO model represents a reversible interaction that is dependent on the gas and solid surface's equilibrium states. The gas forms a covalent link with the adsorbent surface, despite the PSO kinetic model's suggestion that the process of adsorption could include substantial chemical processes [21,22]. According to Blanchard et al. [23], the square of the number of adsorption sites equals the adsorption rate. The following equation might be used to represent the PSO model:

$$\frac{t}{Q_t} = \frac{1}{k_2 {Qe}^2} + \frac{1}{Q_e} t \quad (4)$$

where k_2 is the PSO model's rate constant.

2.5.3 Avrami's Fractional Order model

Avrami's Fractional Order model was first used to investigate the nucleation process of particles [24]. These days, it's common to utilize it to explain the CO_2 sorption process for various adsorbent kinds. This model is being used to investigate the CO_2 adsorption mechanism, which includes chemical and physical adsorption [25-27]. Specific changes in certain kinetic parameters can be verified using this model [28]. Some explanations for Avrami's Fractional Order model are listed below:

$$Q_t = Q_e[1 - e^{-(k_{av}t)^{n_{av}}}] \quad (5)$$

where k_{av} is the Avrami rate constant and n_{av} is the Avrami exponent which is connected to the adsorption mechanism and can be applied to verify any potential interactions that may occur during the adsorption process [29]. The CO_2 adsorption is homogeneous if n_{av} = 1. It is shown that perfect one-dimensional growth exists if n_{av} = 2. The value of three for n_{av} indicates two-dimensional growth. The symbol for three-dimensional growth is n_{av} = 4.

The nonlinear coefficient determination (R^2) was calculated to evaluate the good fit of the three models chosen. The value can be achieved from the graph linear equation to detect the best fit by looking at the R^2 value nearest to 1.

3. Results & Discussion

3.1 Characterization of the Prepared MOF Adsorbents

3.1.1 Surface morphology and composition analyses

Figure 2 presents the SEM images of Fe-MOF (a), Cu-MOF (b), and Fe/Cu-MOF (c) adsorbents, highlighting their distinct surface morphologies. SEM images as shown in Figure 2 reveal irregular aggregated particles rather than well-defined octahedral or cubic crystals typically observed in highly crystalline MOFs [30]. The Fe-

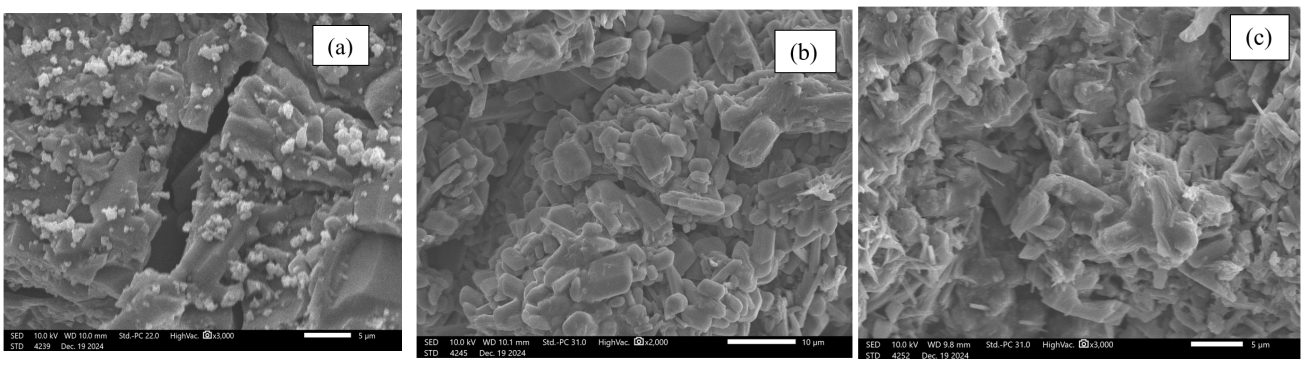

Figure 2. SEM pictures of (a) 3000x Fe-MOF, (b) 2000x Cu-MOF and (c) 3000x Fe/Cu-MOF.

MOF (Figure 2(a)) exhibited sheet-like aggregates, while Cu-MOF (Figure 2(b)) displayed irregular plate- and rod-like morphologies. The bimetallic Fe/Cu-MOF (Figure 2(c)) showed increased agglomeration and heterogeneous particle distribution. The absence of uniform crystal morphology suggests partial framework development or defect-rich coordination structures.

The elemental composition of Fe-MOF, Cu-MOF, and Fe/Cu-MOF is presented in the Energy-Dispersive X-ray spectroscopy (EDX) analysis shown in Table 1. This analysis confirms the presence of key structural elements and highlights differences in the elemental distribution across the various adsorbents. For Fe-MOF, the composition consists predominantly of carbon (46.83%) and oxygen (47.17%), which are likely derived from the organic ligands and metal-oxygen coordination framework. The iron (Fe) content is relatively low at 6%, suggesting a structure where iron is incorporated within an organic framework, possibly as metal clusters or coordination nodes. In the case of Cu-MOF, oxygen (43.06%) and carbon (17.67%) remain major constituents, while copper (Cu) is significantly present at 25.47%, confirming its role as the central metal node in the MOF structure. Additionally, a notable sulfur (S) content of 13.80% is observed in the prepared adsorbent. For the bimetallic Fe/Cu-MOF, the EDX results indicate a more complex composition with Fe (23.44%) and Cu (15.10%) coexisting within the structure, implying a successful incorporation of both metal species into the framework. Oxygen (35.14%) and carbon (13.91%) are present in lower amounts compared to Fe-MOF and Cu-MOF, likely due to structural variations and different ligand interactions.

The presence of sulfur in Cu-MOF and Fe/Cu-MOF likely originates from residual sulfate ions derived from the $CuSO_4$ precursor. Although washing steps were performed, complete removal of sulfate species may not have been achieved. The relatively high sulfur content suggests that residual sulfate species may remain within the material, potentially affecting porosity and structural definition. Thus, the EDX results corroborate the unique structural properties of Fe-MOF, Cu-MOF, and Fe/Cu-MOF by confirming their separate elemental compositions. The balanced mix of Fe and Cu in the bimetallic Fe/Cu-MOF may have synergistic effects in adsorption applications.

Table 1. Chemical compositions of the Fe-MOF, Cu-MOF and Fe/Cu-MOF by EDX.

Adsorbent	Element	Mass %
Fe-MOF	C	46.83
	O	47.17
	Fe	6.000
Cu-MOF	C	17.67
	O	43.06
	Cu	25.47
	S	13.80
Fe/Cu-MOF	Fe	23.44
	Cu	15.10
	O	35.14
	C	13.91
	S	12.40

3.1.2 Surface area analysis

The N_2 adsorption-desorption isotherms measured at 77 K revealed relatively low BET surface areas for all synthesized materials, with values of 4.3 $m^2.g^{-1}$ for Cu-MOF, 11.1 $m^2.g^{-1}$ for Fe-MOF, and 19.4 $m^2.g^{-1}$ for Fe/Cu-MOF as shown in Figure 3 and Table 2.

These values are significantly lower than those commonly reported for highly crystalline microporous MOFs, which often exhibit surface areas exceeding 1000 $m^2\ g^{-1}$. The substantial difference indicates that the prepared materials possess limited N_2-accessible porosity under the applied measurement conditions. One possible explanation is incomplete solvent removal during the activation process. MOF porosity is highly dependent on effective activation to remove trapped synthesis solvents, particularly high-boiling-point solvents such as DMF. In this study, the materials were washed with methanol and

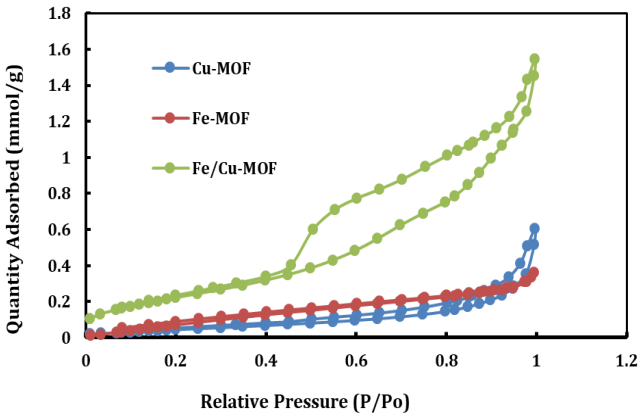

Figure 3. N_2 adsorption-desorption isotherms for Cu-MOF, Fe-MOF and Fe/Cu-MOF.

Table 2. The prepared adsorbents' surface area, pore size, and pore volume as evaluated by BET analysis.

Sample	BET surface area ($m^2.g^{-1}$)	Pore size (Å)	Pore volume ($cm^3.g^{-1}$)
Cu-MOF	4.3355	91.808	0.013911
Fe-MOF	11.1253	45.826	0.016319
Fe/Cu-MOF	19.3989	78.790	0.048991

dried under vacuum at 120 °C, however, no prolonged solvent exchange or gradual activation protocol was implemented. Residual DMF molecules can strongly coordinate to metal centers and remain confined within pore cavities. If these molecules are not fully removed prior to BET analysis, they may block micropore entrances, reduce accessible pore volume, and suppress N_2 diffusion at 77 K. Since nitrogen adsorption at cryogenic temperature is diffusion-sensitive [30], even partial pore obstruction can substantially reduce the measured surface area.

Another contributing factor may be partial pore blockage by residual inorganic species. Elemental analysis revealed measurable sulfur content in the Cu-MOF and Fe/Cu-MOF samples. Because copper sulfate ($CuSO_4 \cdot 5H_2O$) was used as the copper precursor, residual sulfate ions may remain within the framework if washing was incomplete. Sulfate anions are relatively large and strongly coordinating; if retained within the structure, they may occupy pore cavities, adsorb onto metal nodes, or form secondary inorganic domains [31]. Such residual species can obstruct pore channels and reduce effective pore connectivity, thereby decreasing N_2-accessible surface area while still allowing limited surface adsorption behavior.

It is also possible that the reaction conditions favored the formation of dense coordination networks rather than fully developed three-dimensional microporous MOF architectures. Instead of forming highly ordered frameworks comparable to classical MIL- or HKUST-type structures, the materials may consist of layered, sheet-like, or partially cross-linked coordination assemblies. Such structures can still contain accessible metal sites and surface adsorption domains but may lack the interconnected microporous channels necessary for high nitrogen uptake at cryogenic temperature. The SEM images (Figure 2) showing aggregated and sheet-like morphologies support this interpretation.

Despite the overall low BET surface areas, the Fe/Cu-MOF sample exhibited the highest pore volume (0.0489 $cm^3.g^{-1}$) and the largest surface area among the three materials. This suggests that bimetallic incorporation may have introduced additional structural heterogeneity or improved pore connectivity relative to the single-metal analogues. The presence of two different metal centers can influence nucleation and crystal growth behavior, potentially generating microstructural voids and more accessible surface regions [32]. Although the absolute surface area values remain low, the relative enhancement observed for Fe/Cu-MOF indicates a beneficial structural effect arising from bimetallic synergy. Thus, the low measured surface areas suggest that the synthesized materials possess moderate porosity and partially developed framework structures rather than classical high-surface-area microporous MOFs. The combination of possible incomplete activation, residual sulfate species, structural defects, and dense coordination domains likely contributes to the limited nitrogen-accessible porosity.

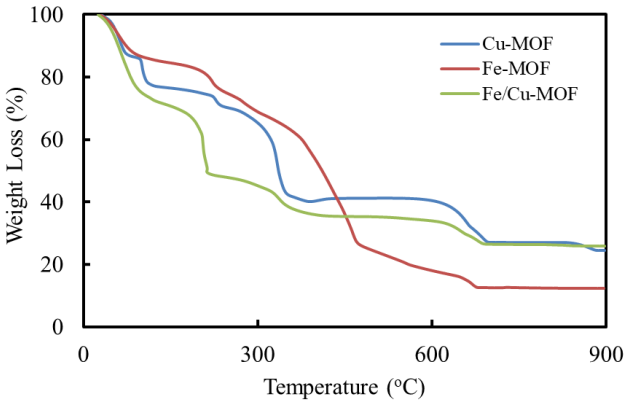

Figure 4. TGA curves for Fe-MOF, Cu-MOF and Fe/Cu-MOF.

3.1.3 Thermal Gravimetric Analysis (TGA)

The TGA curves of Cu-MOF, Fe-MOF, and Fe/Cu-MOF are shown in Figure 4, providing information about their thermal characteristics. Of the three, Cu-MOF has the best thermal stability; as the temperature rises, a progressive weight loss is observed. This material maintains its structural integrity up to relatively high temperatures before significant disintegration occurs, likely in several stages, due to the loss of solvent molecules, organic linkers, and eventual framework collapse. Cu-MOF demonstrates excellent thermal stability, making it ideal for applications that require resistance to high temperatures. In contrast, Fe-MOF loses weight at lower temperatures, indicating reduced thermal stability. This suggests that Fe-MOF may decompose more easily, especially after losing volatile components such as water. As a result, Fe-MOF is less suitable for high-temperature applications compared to Cu-MOF. On the other hand, Fe/Cu-MOF shows intermediate thermal stability, with its decomposition behavior falling between Cu-MOF and Fe-MOF. The combination of iron and copper likely contributes to a more complex degradation process, which may involve multiple stages of weight loss. Thus, Fe/Cu-MOF offers a balanced option for applications that require moderate thermal stability, combining thermal resistance with other functional properties.

3.1.4 Functional group analysis

The FTIR spectra of Fe-MOF, Cu-MOF, and Fe/Cu-MOF, presented in Figure 5, highlight distinct differences in their molecular interactions and structural characteristics. The

characteristic absorption bands observed in Cu-MOF are associated with the vibrations of its metal-oxygen bonds and the organic linkers. For example, bands about 500-700 cm^{-1} may correspond to Cu-O stretching modes, whereas peaks in the 1500-1600 cm^{-1} range are usually associated with C=O stretching vibrations. These characteristics show that the Cu-MOF structure contains organic components and clearly defined coordination bonds. However, Fe-MOF exhibits absorption bands that are characteristic of Fe-O vibrations, which are usually seen in the lower wavenumber range (below 600 cm^{-1}). Furthermore, Fe-MOF may exhibit hydroxyl group (O-H stretching) peaks at 3200-3600 cm^{-1}, indicating the presence of hydroxyl or water species within its structure. This is in line with iron-based MOFs' propensity to absorb moisture.

Fe/Cu-MOF, as a hybrid material, combines features from both Fe-MOF and Cu-MOF. Its spectrum shows overlapping peaks corresponding to both Fe-O and Cu-O vibrations, as well as the organic linker vibrations. The presence of both metal centers in Fe/Cu-MOF likely results in a more complex spectrum, with additional peaks or shifts due to interactions between iron and copper within the framework. For example, the C=O stretching region may show slight shifts compared to pure Cu-MOF, indicating altered electronic environments due to the incorporation of iron.

3.1.5 Surface structure analysis

Figure 6 depicts the XRD spectra of Cu-MOF, Fe-MOF and Fe/Cu-MOF adsorbents. X-ray diffraction analysis confirmed the formation of crystalline coordination structures in all synthesized materials. Distinct diffraction peaks were observed in the patterns of Cu-MOF, Fe-MOF, and Fe/Cu-MOF, indicating that metal-ligand coordination reactions occurred during the solvothermal synthesis. The presence of identifiable reflections suggests that the adsorbents are not entirely amorphous precipitates but contain ordered domains characteristic of coordination frameworks.

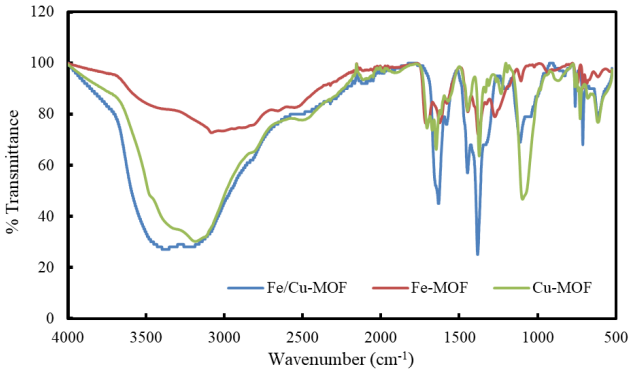

Figure 5. FTIR spectrum of Fe-MOF, Cu-MOF and Fe/Cu-MOF.

However, the diffraction peaks exhibit noticeable broadening and moderate intensities, particularly in the Fe-MOF sample. Peak broadening in XRD patterns is commonly associated with small crystallite size, lattice strain, structural disorder, or the presence of defects within the framework [33]. Reduced peak intensity and partial baseline elevation further suggest limited long-range periodicity. In highly crystalline MOFs, sharp and intense reflections are typically observed due to well-defined and repetitive pore architectures. In contrast, the broadened peaks observed here indicate that while short-range coordination order exists, the materials likely lack extensive long-range structural regularity. The Fe-MOF sample shows the most pronounced peak broadening, which may reflect a semi-crystalline or defect-rich framework. Iron-based MOFs are known to be sensitive to synthesis conditions, and rapid nucleation or non-ideal stoichiometry can promote the formation of poorly ordered coordination networks. Additionally, iron centers often exhibit flexible coordination geometries, which can result in structural distortion and reduced crystallinity [34]. These factors may contribute to the limited structural ordering observed in the Fe-MOF pattern.

The Cu-MOF sample demonstrates comparatively sharper and more defined peaks than Fe-MOF, suggesting relatively improved structural organization. Copper typically forms more rigid paddle-wheel secondary building units in many classical MOF structures, which may promote better ordering during crystal growth. Nevertheless, the diffraction pattern does not fully correspond to that of well-known Cu-based benchmark materials such as HKUST-1. In particular, the characteristic high-intensity reflections commonly reported for highly crystalline HKUST-type frameworks are not clearly reproduced. This discrepancy suggests that although coordination between copper ions and organic linkers occurred, the resulting structure may differ from classical topologies or may contain significant structural defects.

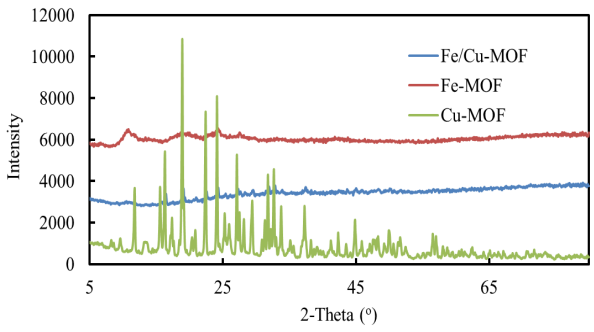

Figure 6. Cu-MOF, Fe-MOF and Fe/Cu-MOF XRD spectra.

The bimetallic Fe/Cu-MOF sample exhibited improved crystallinity compared to Fe-MOF, as evidenced by relatively sharper diffraction peaks and enhanced intensity at certain 2θ positions. The incorporation of copper alongside iron may have influenced nucleation kinetics and framework assembly, promoting improved structural organization. Bimetallic systems can alter crystal growth behavior by balancing coordination geometries and stabilizing intermediate structural motifs [35]. This may explain the moderate enhancement in crystallinity observed in the Fe/Cu-MOF pattern.

However, despite this relative improvement, the diffraction pattern of Fe/Cu-MOF does not fully match those of highly crystalline MIL-series or HKUST-type materials reported in the literature. The absence of strong, well-resolved reflections across the full 2θ range suggests that the material likely consists of partially ordered domains rather than a fully developed three-dimensional microporous lattice. Furthermore, the presence of moderate peak broadening indicates that crystallite size may be small or that structural defects are present within the framework. It is also important to consider that residual inorganic species, such as sulfate derived from the copper precursor, may influence diffraction features. The incorporation or retention of sulfate ions could introduce secondary phases or lattice distortion, contributing to peak broadening and reduced crystallinity. Additionally, partial pore collapse during drying or incomplete solvent removal may induce structural contraction, further diminishing long-range order [36].

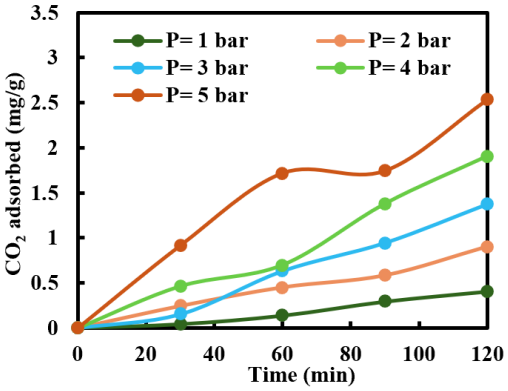

(a)

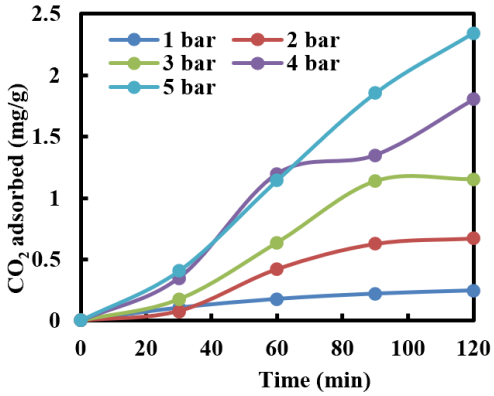

(b)

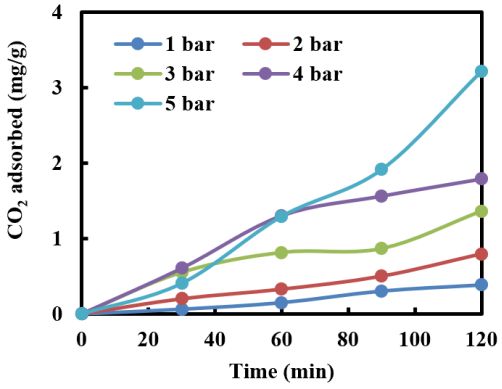

(c)

Figure 7. Effect of pressure on CO_2 adsorption using Fe-MOF (a), Cu-MOF (b) and Fe/Cu-MOF (c) adsorbents.

Taken together, the XRD results indicate that the synthesized materials contain crystalline coordination domains but do not exhibit the highly ordered, extended periodicity typical of fully optimized microporous MOFs. The diffraction behavior suggests partially crystalline coordination frameworks with limited long-range structural regularity. This interpretation is consistent with the BET analysis, which revealed limited nitrogen-accessible surface area. The combined structural evidence therefore supports the conclusion that the materials represent moderately ordered coordination networks rather than classical high-surface-area MOF architectures.

3.2 CO_2 Adsorption

3.2.1 Effect of pressure

The influence of operating pressure on CO_2 adsorption was investigated between 1 and 5 bar at 303 K for Fe-MOF, Cu-MOF, and Fe/Cu-MOF. As shown in Figure 7, all adsorbents exhibit a clear pressure-dependent increase in adsorption capacity, confirming that elevated pressure substantially enhances CO_2 uptake. For Fe-MOF, the adsorption capacity increased from 0.405 $mg.g^{-1}$ at 1 bar to 2.535 $mg.g^{-1}$ at 5 bar after 120 min, corresponding to an approximately six-fold enhancement. A similar trend was observed for Cu-MOF, where adsorption rose from 0.245 $mg.g^{-1}$ to 2.347 $mg.g^{-1}$ across the same pressure range. The bimetallic Fe/Cu-MOF displayed the strongest pressure response, with CO_2 uptake increasing from 0.385 $mg.g^{-1}$ at 1 bar to 3.22 $mg.g^{-1}$ at 5 bar, representing the highest adsorption capacity among all materials.

This pronounced increase in CO_2 uptake with pressure is attributed to the elevated gas-phase CO_2 density, which enhances the chemical

potential gradient between the bulk gas and the adsorbent surface. Higher pressure increases molecular collision frequency and facilitates diffusion of CO_2 into accessible pores, thereby promoting progressive site occupation and pore filling [37]. At low pressures (1-2 bar), adsorption proceeds slowly due to limited driving force, while at higher pressures (3-5 bar), uptake accelerates markedly as additional adsorption domains become accessible. The superior pressure sensitivity of Fe/Cu-MOF is strongly supported by the characterization results. BET analysis revealed that Fe/Cu-MOF possesses the highest surface area (19.4 $m^2.g^{-1}$) and pore volume (0.0489 $cm^3.g^{-1}$), exceeding those of Fe-MOF (11.1 $m^2.g^{-1}$; 0.0163 $cm^3.g^{-1}$) and Cu-MOF (4.3 $m^2.g^{-1}$; 0.0139 $cm^3.g^{-1}$). Although the absolute BET values are modest, the relatively larger pore volume of Fe/Cu-MOF provides greater capacity for pressure-assisted pore filling, explaining its enhanced uptake at elevated pressures.

EDX and FTIR analyses further confirm the coexistence of Fe and Cu within the bimetallic framework, generating chemically heterogeneous adsorption sites. This dual-metal environment increases the diversity and density of CO_2-binding domains, enabling stronger metal-CO_2 interactions compared with single-metal MOFs. XRD patterns show improved crystallinity of Fe/Cu-MOF relative to Fe-MOF, suggesting better pore connectivity and reduced transport resistance, which further facilitates CO_2 diffusion under pressurized conditions. In contrast, Cu-MOF exhibits the weakest pressure response, consistent with its lowest BET surface area and evidence of residual sulfate species from the $CuSO_4$ precursor observed in EDX analysis. These residues likely partially block pore channels and reduce effective adsorption site availability, limiting the extent of pressure-driven uptake. Fe-MOF shows intermediate behavior, reflecting moderate surface area but greater structural disorder, as indicated by broader XRD peaks.

Notably, appreciable CO_2 adsorption is achieved despite low N_2-accessible surface areas, highlighting the limitation of nitrogen physisorption in predicting CO_2 capture performance. CO_2 possesses a smaller kinetic diameter and a significant quadrupole moment, enabling preferential interaction with open metal sites, defect regions, and mesoporous surfaces that may be inaccessible to N_2 at 77 K. Consequently, adsorption in these materials likely proceeds through a combination of surface coordination, defect-site adsorption, and pressure-induced pore filling rather than classical micropore confinement alone. Thus, increasing pressure significantly enhances CO_2 adsorption for all synthesized MOFs, with performance following the order of Fe/Cu-MOF > Fe-MOF > Cu-MOF. The results demonstrate that bimetallic incorporation markedly improves pressure-dependent adsorption through synergistic effects on pore structure, crystallinity, and active site chemistry, establishing Fe/Cu-MOF as the most promising candidate for pressurized CO_2 capture applications.

3.2.2 Effect of dosages

The effect of adsorbent dosage on CO_2 adsorption using Fe-MOF, Cu-MOF and Fe/Cu-MOF adsorbents is depicted in the Figure 8, where different masses (0.2-0.5 g) are evaluated over a period of 120 minutes. The effect of adsorbent dosage on CO_2 adsorption was examined by varying the mass from 0.2 to 0.5 g at constant pressure and temperature. Figure 8 illustrates the adsorption behavior of Fe-MOF, Cu-MOF, and Fe/Cu-MOF over 120 min. For all adsorbents,

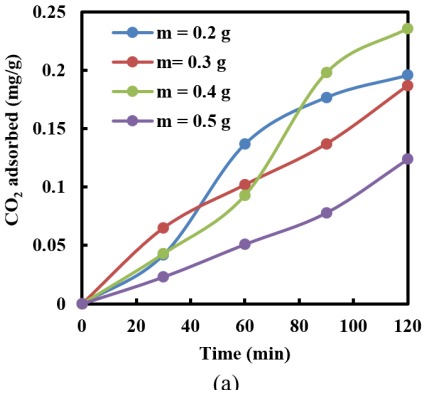

(a)

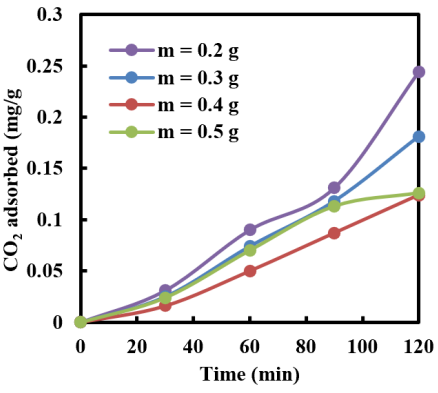

(b)

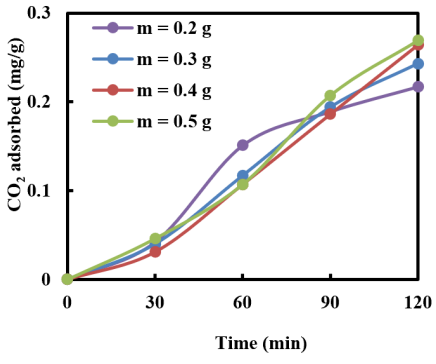

(c)

Figure 8. Effect of adsorbent dosage on CO_2 adsorption using Fe-MOF (a), Cu-MOF (b) and Fe/Cu-MOF (c) adsorbents.

increasing dosage enhanced total CO_2 removal; however, the normalized adsorption capacity (mg g^{-1}) exhibited non-linear trends, indicating that adsorption efficiency is governed not only by adsorbent quantity but also by site accessibility and gas-solid mass transfer limitations.

For Fe-MOF, the adsorption capacity increased from 0.196 $mg.g^{-1}$ at 0.2 g to a maximum of 0.236 $mg.g^{-1}$ at 0.4 g, before declining sharply to 0.124 $mg.g^{-1}$ at 0.5 g. This non-monotonic behavior suggests that 0.4 g represents an optimal dosage, providing a balance between sufficient adsorption sites and effective gas accessibility. The reduced performance at 0.5 g is attributed to particle agglomeration and bed compaction, which limit CO_2 diffusion into internal adsorption domains, as supported by SEM images showing aggregated Fe-MOF morphologies.

Cu-MOF displayed consistently lower adsorption capacities across all dosages, reaching 0.244, 0.181, 0.124, and 0.126 $mg.g^{-1}$ at 0.2, 0.3, 0.4, and 0.5 g, respectively, after 120 min. The decline in normalized uptake with increasing dosage reflects restricted pore accessibility and reduced utilization of active sites. This behavior correlates with BET results, which revealed Cu-MOF to possess the lowest surface area (4.3 $m^2.g^{-1}$) and pore volume, as well as EDX evidence of residual sulfate species that may partially block pore channels and suppress adsorption efficiency.

In contrast, Fe/Cu-MOF exhibited the highest overall adsorption performance, with capacities increasing from 0.217 $mg.g^{-1}$ at 0.2 g to 0.269 $mg.g^{-1}$ at 0.5 g. Unlike Fe-MOF and Cu-MOF, Fe/Cu-MOF showed a more gradual and monotonic improvement with dosage, indicating more effective utilization of additional adsorbent mass. This superior behavior is consistent with its higher BET surface area (19.4 $m^2.g^{-1}$) and pore volume (0.0489 $cm^3.g^{-1}$), as well as the presence of dual metal centers confirmed by EDX and FTIR. The bimetallic framework provides chemically heterogeneous adsorption sites and improved pore connectivity, as evidenced by XRD, facilitating enhanced CO_2 diffusion and adsorption even at higher loadings. At low dosages, higher gas-to-solid ratios favor rapid adsorption kinetics, while at higher dosages, gas-phase limitation and interparticle diffusion resistance become dominant, leading to diminishing returns in normalized capacity. These findings indicate that CO_2 adsorption in the present system is controlled by a combination of available adsorption sites, pore accessibility, and mass transfer efficiency rather than adsorbent mass alone.

3.2.3 Effect of temperature

The effect of temperature on CO_2 adsorption was evaluated at 40, 45, and 50 °C under constant pressure at 1 bar and 0.2 g of adsorbent mass for Fe-MOF, Cu-MOF, and Fe/Cu-MOF. The adsorption capacities derived from concentration decay profiles are presented in Figure 9. For all three adsorbents, CO_2 uptake decreased with increasing temperature, confirming that adsorption is predominantly exothermic in nature. At 120 min, Fe-MOF exhibited adsorption capacities of 0.226, 0.195, and 0.213 $mg.g^{-1}$ at 40, 45, and 50 °C, respectively. Cu-MOF showed corresponding values of 0.231, 0.191, and 0.184 $mg.g^{-1}$, while Fe/Cu-MOF demonstrated the highest overall adsorption with capacities of

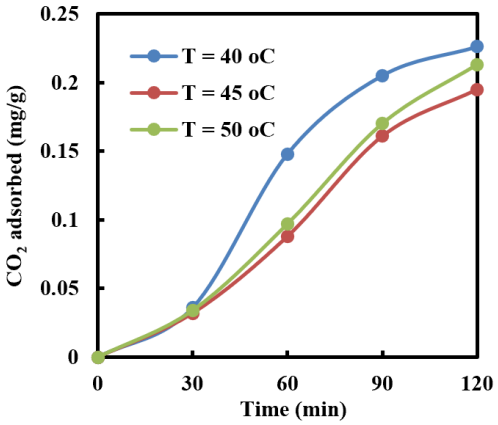

(a)

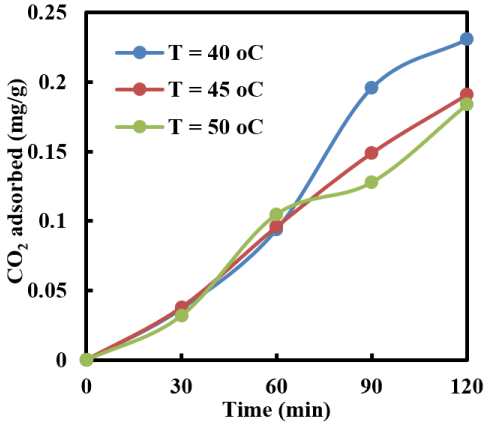

(b)

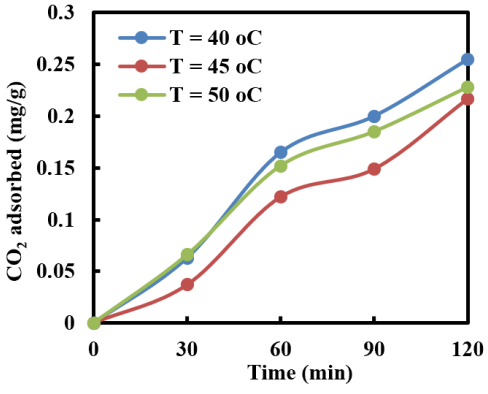

(c)

Figure 9. Temperature-dependent behavior of CO_2 adsorption using Fe-MOF (a), Cu-MOF (b) and Fe/Cu-MOF (c) adsorbents.

0.255, 0.217, and 0.228 $mg.g^{-1}$. The maximum adsorption for all materials occurred at 40 °C, indicating that lower temperatures favor CO_2 capture. As temperature increases, the kinetic energy of CO_2 molecules rises, weakening adsorbate-adsorbent interactions and promoting desorption, thereby reducing net uptake. This behavior is characteristic of physisorption-dominated systems, where adsorption is driven primarily by van der Waals forces and electrostatic interactions rather than strong chemical bonding [38].

Among the three materials, Fe/Cu-MOF consistently exhibited superior adsorption performance across all temperatures. This enhancement is attributed to its higher BET surface area (19.4 $m^2.g^{-1}$) and pore volume (0.0489 $cm^3.g^{-1}$), as well as the presence of dual metal centers confirmed by EDX and FTIR analyses. The coexistence of Fe and Cu generates chemically heterogeneous adsorption sites, increasing CO_2 affinity and providing multiple binding environments. In addition, XRD results indicate improved crystallinity of Fe/Cu-MOF compared with Fe-MOF, suggesting better pore connectivity and reduced diffusion resistance, which collectively contribute to its higher temperature-tolerant adsorption behavior.

These results demonstrate that CO_2 adsorption in the present system is governed by exothermic physisorption, and that bimetallic Fe/Cu incorporation effectively mitigates temperature-induced performance losses by enhancing pore structure and active site availability.

3.3 CO_2 Adsorption Kinetic Study

The CO_2 adsorption rate, which regulates the adsorption reaction time, is defined by the adsorption kinetics. It is among the key elements in determining the adsorption efficiency over a certain time frame. Plots from the Avrami kinetics model, Pseudo-first order (PFO), and Pseudo-second order (PSO) models are shown in Figure 10 of this work. These models have been studied by utilizing experimental data for CO_2 adsorption with various solid adsorbent-based MOFs. Table 3 contains all the kinetic parameters that were determined by fitting model plots. The most appropriate model for the data was chosen using the linear regression coefficient correlation (R^2) values. According to a comparison of their R^2 values, kinetic models fitted in the following order: PFO>PSO>Avrami. This indicates that the CO_2 adsorption process is best described by the PFO kinetic model. Thus, the CO_2 adsorption mechanism is physisorption throughout the adsorption process employing solid adsorbents-based MOFs, where CO_2 molecules must first be adsorbed on the solid adsorbent's exterior to execute CO_2 adsorption.

Adsorption tests were conducted with the following parameters: 0.2 g of adsorbent, 5 bars of pressure, and reaction temperature at ambient condition. As demonstrated by Table 3, the kinetic constants (k) for Fe/Cu-MOF shows the highest value for all the kinetic models employed. With the combination of both metals positively promotes the adsorption rate. The results displayed in Figure 10 and Table 3 reveal that the primary mechanism of CO_2 adsorption is physisorption, in which the gas atom interacts with the adsorbent's surface characteristics. As shown in Table 2, the additional secondary metal in the bimetal-MOF results in an enhance BET surface area than in the mono-MOF. The introduction of the second metal to the mono-MOF does change the original morphology and slightly increase the size of the particle because of the rise of the second ion content. The raised amount of the metal ions added into the framework produce tinier pores. Apart from that, the amount of the second metal introduced should have to be compatible in terms of Coulombic charges and ionic sizes of the host metal. The amount of not compatible with the host metal can damage the adsorption rate. Other than that, in the bimetallic

Table 3. PFO, PSO, and Avrami's Fractional Order Models' kinetic parameters under different adsorbents-based MOFs.

Kinetic model	Adsorbent	Parameter		
		Kinetic rate constant, k	R^2	n_{av}
PFO	Fe/Cu-MOF	0.026	0.8341	
	Fe-MOF	0.0223	0.8251	-
	Cu-MOF	0.0256	0.9727	
PSO	Fe/Cu-MOF	0.000175	0.6267	
	Fe-MOF	0.000163	0.6467	-
	Cu-MOF	0.000155	0.7272	
Avrami	Fe/Cu-MOF	0.0319	0.7217	0.9616
	Fe-MOF	0.0216	0.5849	0.6634
	Cu-MOF	0.0242	0.9124	0.8987

MOF, the amount of the inserted second metal must not exceed the certain amount that could lead to blockage of the ions on the metal sites in the MOF due to the internal pores of the MOF having been filled with the second ion.

Furthermore, Table 3, which evaluates Avrami's exponent n_{av} based on its fractional order, demonstrates that the adsorption is homogeneous because it approaches 1 for Fe/Cu-MOF. However, increased molecular mobility at already-existing adsorption sites leads to heterogeneous adsorption as the kinetic constant increases. As was previously indicated, the CO_2 adsorption mechanism, which combines chemical

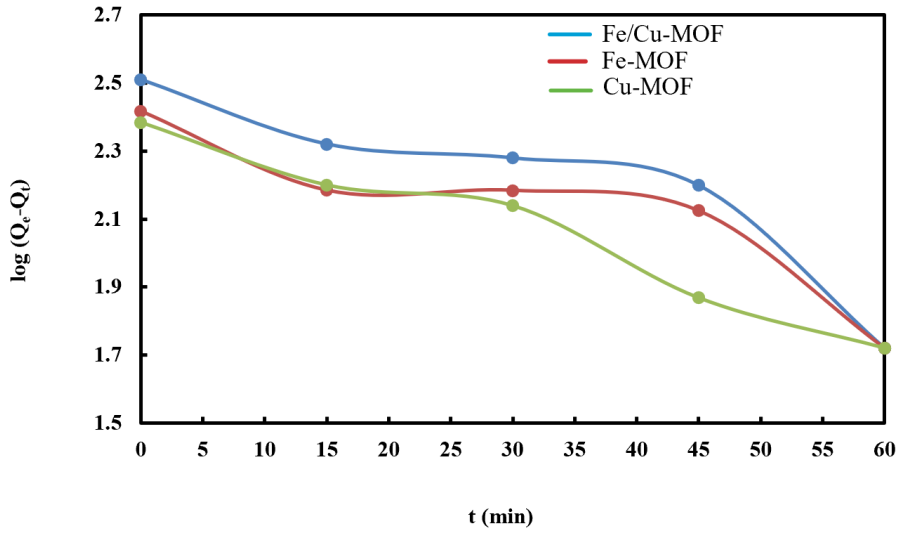

(a)

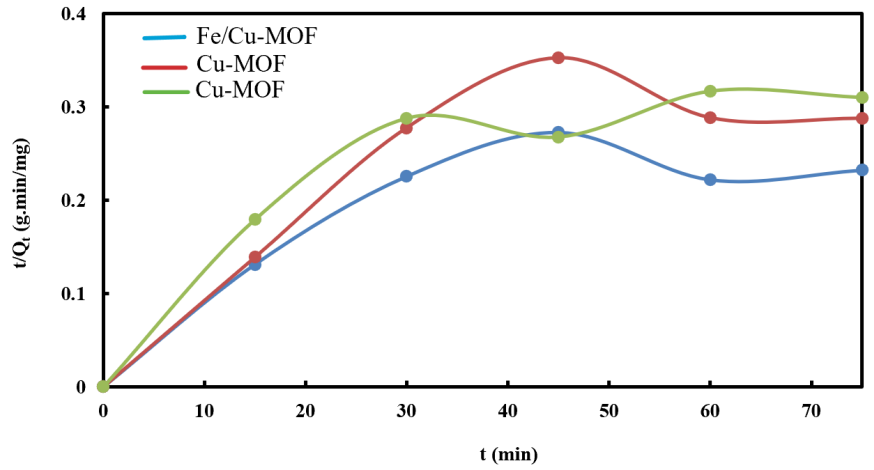

(b)

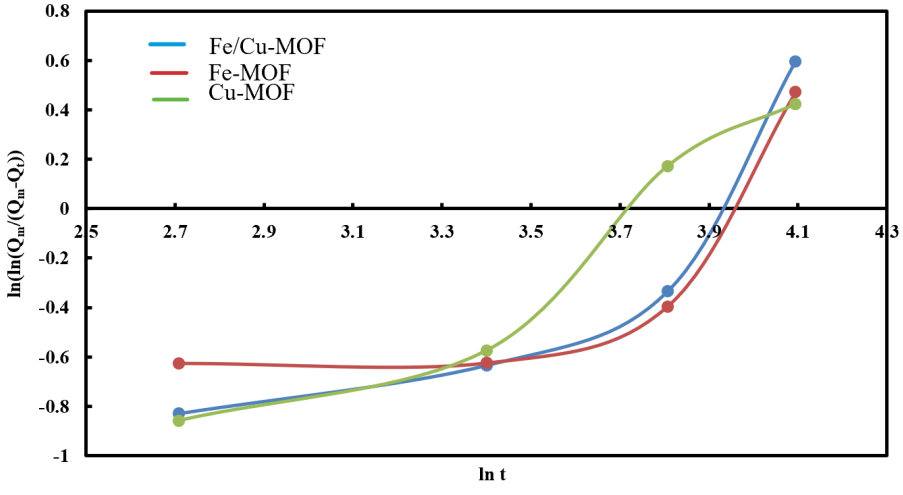

(c)

Figure 10. Comparison of different kinetic models for CO_2 adsorption using solid adsorbent-based MOFs employing (a) PFO, (b) PSO, and (c) Avrami's fractional kinetic model.

and physical adsorption, is revealed using Avrami's fractional order [39]. As a result, it can be concluded that the PFO is best suited to predict the adsorption behavior of solid adsorbent-based MOFs.

4. Conclusions

Fe-MOF, Cu-MOF, and bimetallic Fe/Cu-MOF were synthesized and comparatively evaluated for CO_2 adsorption under controlled pressure, dosage, and temperature conditions. Structural characterization revealed partially crystalline, defect-rich coordination frameworks with relatively low N_2-accessible surface areas; however, Fe/Cu-MOF exhibited the highest BET surface area (19.4 $m^2.g^{-1}$) and pore volume (0.0489 $cm^3.g^{-1}$), together with improved crystallinity and dual-metal active sites. These features translated directly into superior adsorption performance. CO_2 uptake increased significantly with pressure for all materials, with Fe/Cu-MOF achieving the highest capacity of 3.22 $mg.g^{-1}$ at 5 bar, confirming the strong influence of gas-phase driving force and pressure-assisted pore filling. Dosage studies revealed non-linear behavior, where excessive adsorbent loading led to site underutilization and diffusion resistance, while temperature-dependent experiments demonstrated decreased adsorption at elevated temperatures, consistent with exothermic physisorption. Kinetic analysis indicated that CO_2 adsorption follows a pseudo-first-order model, highlighting surface-controlled uptake. Overall, adsorption performance followed the order Fe/Cu-MOF > Fe-MOF > Cu-MOF, demonstrating that bimetallic incorporation provides a clear advantage through synergistic enhancement of pore structure, adsorption site heterogeneity, and mass-transfer accessibility. Although the synthesized materials exhibit moderate surface areas compared with benchmark MOFs, appreciable CO_2 capture was achieved due to defect-assisted adsorption and metal-CO_2 interactions. These results establish Fe/Cu-MOF as a promising low-cost bimetallic adsorbent for pressurized CO_2 capture and offer valuable insight for designing next-generation MOFs with improved adsorption efficiency via controlled structural heterogeneity and multi-metal coordination.

Acknowledgment

The Universiti Malaysia Pahang Al-Sultan Abdullah provided funding for this work through the Research Grant (Grant No.: RDU250318). For the technical assistance and research facilities offered during the study, the authors further sincerely thank the Faculty of Chemical and Process Engineering Technology at Universiti Malaysia Pahang Al-Sultan Abdullah (UMPSA).

CRedit Author Statement

Author Contributions: N.K. Daud: Conceptualization, Methodology, Investigation, Resources, Data Curation, Writing, Review and Editing, Supervision; H. Abdullah: Conceptualization, Methodology, Formal Analysis, Data Curation, Writing Draft Preparation, Visualization, Software, Project Administration; N. A. Ismail: Validation, Writing, Review and Editing, Data Curation. All authors have read and agreed to the published version of the manuscript.

References

[1] Li, J.R., Sculley, J., Zhou, H.C. (2012). Metal-Organic Frameworks for Separations. *Chemical Reviews,* 112(2), 869-932. DOI: 10.1021/cr200190s

[2] Sumida, K., Rogow, D.L., Mason, J.A., McDonald, T.M., Bloch, E.D., Herm, Z.R., Bae, T.H., Long, J.R. (2012). Carbon Dioxide Capture in Metal-Organic Frameworks. *Chemical Reviews*, 112(2), 724-781. DOI: 10.1021/cr2003272

[3] Zhou, H.C., Long, J.R., Yaghi, O.M. (2012). Introduction to Metal-Organic Frameworks. *Chemical Reviews*, 112(2), 673-674. DOI: 10.1021/cr300014x

[4] Liu, J., Wang, Y., Benin, A.I., Jakubczak, P., Lanuza, M., Willis, R.R., LeVan, M.D. (2010). CO_2/H_2O Adsorption Equilibrium and Rates on Metal-Organic Frameworks: HKUST-1 and Ni/DOBDC. *Langmuir*, 26(20), 14301-14307. DOI: 10.1021/la102359q

[5] Li, H., Xu, C., Li, N., Tao, R., Zhong, Z., Zhou, Q., Wang, C., Xu, S., Tang, J. (2022). Synthesis of Bimetallic FeCu-MOF and Its Performance as Catalyst of Peroxymonosulfate for Degradation of Methylene Blue. *Materials*, 15(20), 1-16. DOI: 10.3390/ma15207252

[6] Thi, C.Q.N., Thi, N.D.N., Hung, D.C., Bich, N.H. (2023). Evaluation of the Effect of Bimetallic Organic Framework M/Fe-MOF (M=Ni, Co) on the Removal of Congo Red Dye. P*olish Journal of Environmental Studies*, 2(32), 2-10. DOI: 10.15244/pjoes/155874

[7] Zeng, X., Zhang, G., Zhu, J. (2022). Selective adsorption of heavy metals from water by a hyper-branched magnetic composite material: Characterization, performance, and mechanism. *Journal of Environmental Management,* 314, 114979. DOI: 10.1016/j.jenvman.2022.114979

[8] Yang, X., Qin, J., Dai, Z., Sun, Y., Liu, H, Zheng, X., Hu, Z. (2023). MOF-derived Fe based catalysts for efficiently Advanced Oxidation Processes: From single atoms to diatomic and nanoparticles. *Progress in Natural Science: Materials International*, 33(4), 534-543. DOI: 10.1016/j.pnsc.2023.10.002

[9] Elena, G.R., Jesús, T., Pedro, L., Carmen, M., Gisela, O. (2025). Synergistic performance of novel Cu-MOF-74@SBA-15 material in enhanced CO_2 adsorption and transformation. *Journal of CO_2 Utilization*, 92, 103025. DOI: 10.1016/j.jcou.2025.103025

[10] Furukawa, H., Cordova, K.E., O'Keeffe, M., Yaghi, O.M. (2013). The Chemistry and Applications of Metal-Organic Frameworks. *Science*, 341(6149), 1230444. DOI: 10.1126/science.1230444

[11] Xiao, J., Shiya, Y., Hengshuo, H., Shuyu, L., Wenfu, X., Min, L., Tianyu, Z., Qiang, W. (2025). Regulation of Cu-MOF reconstruction for enhanced CO_2 electroreduction. *Applied Catalysis B: Environment and Energy*, 375, 125412. DOI: 10.1016/j.apcatb.2025.125412

[12] Mehrdad, H., Mohammad, R., Federico, G. (2023). Synthesis and characterization of iron incoporated metal-organic framework (MOF) photocatalyst in degradation of methylene blue. *Journal of Water and Environmental Nanotechnology*, 8(1), 1-12. DOI: 10.22090/jwent.2023.08.001

[13] Keaoleboga, M., Mike, M., Guoming, W., Nicholas, M.M., Henrietta, W. (2025). Recent advances in Fe-based metal-organic frameworks: Structural features, synthetic strategies and applications. *Coordination Chemistry Reviews*, 529, 216467. DOI: 10.1016/j.ccr.2025.216467

[14] Abid, H.S., Zain, U.A., Sumaira, M., Farzana, R., Rafi, U., Attiq, U.R., Muhammad, D., Manzoor, A., Kifayat, U., Muhammad, N.R., Fei, T. (2023). Porous Cu-based metal organic framework (Cu-MOF) for highly selective adsorption of organic pollutants. *Journal of Solid State Chemistry*, 322, 123935. DOI: 10.1016/j.jssc.2023.123935

[15] Wang, F.X, Zhang, Z.W., Fei, W., Ya, L., Zhang, Z. C., Chong, C.W., Baoyi, Y., Xuedong, D., Peng, W., Huifen, F., Chen, Z. (2023). Fe-Cu bimetal metal-organic framework for efficient decontamination via Fenton-like process: Synthesis, performance and mechanism. *Journal of Colloid and Interface Science*, 649, 384-393. DOI: 10.1016/j.jcis.2023.06.083

[16] Antía, F.S., Emilio, R., Marta, P., Angeles, S. (2025). One-pot synthesis of bimetallic Fe-Cu metal-organic frameworks composite for the elimination of organic pollutants via peroxymonosulphate activation. *Environmental Science and Pollution Research*, 32, 10592-10607. DOI: 10.1016/j.jcis.2023.06.083

[17] Noor, K., Nadir, A., Honghai, Y., Wang, J. (2024). Review of MOFs and their applications in the preparation of loose nanofiltration membranes for dye and salt fractionation. *Desalination and Water Treatment*, 317, 100092. DOI: 10.1016/j.dwt.2024.100092

[18] Keaoleboga, M., Mike, M., Guoming, W., Nicholas, M.M., Henrietta, W.L. (2025). Recent advances in Fe-based metal-organic frameworks: Structural features, synthetic strategies and applications. *Coordination Chemistry Reviews*, 529, 216467. DOI: 10.1016/j.ccr.2025.216467

[19] Daud, N.K., Abas, F.N., Najib, N.H.I.M. (2023). CO_2 Adsorption Performance of AC and Zn-MOF for the application of Carbon Capture and Sequestration (CCS). *Materials Today Proceeding*, 1-7. DOI: 10.1016/j.matpr.2023.03.231

[20] Kaur, S., Rani, S., Mahajan, R.K., Asif, M., Gupta, V.K. (2015). Synthesis and adsorption properties of mesoporous material for the removal of dye safranin: kinetics, equilibrium, and thermodynamics. *Journal of Industrial and Engineering Chemistry*, 22, 19–27. DOI: 10.1016/j.jiec.2014.06.019

[21] Loganathan, S., Tikmani, M., Edubilli, S., Mishra, A., Ghoshal, A.K. (2014). CO_2 adsorption kinetics on mesoporous silica under wide range of pressure and temperature. *Chemical Engineering Journal*, 256, 1–8. DOI: 10.1016/j.cej.2014.06.091

[22] Serna-Guerrero, R., Sayari, A. (2010). Modeling adsorption of CO_2 on amine-functionalized mesoporous silica. 2: kinetics and breakthrough curves. *Chemical Engineering Journal,* 161, 182–190. DOI: 10.1016/j.cej.2010.04.042

[23] Blanchard, M.M.G., Martin, G. (1984). Removal of heavy metals from waters by means of natural zeolites, water. *Water Research*, 18, 1501–1507. DOI: 10.1016/0043-1354(84)90124-6

[24] Avrami, M. (1939). Kinetics of phase change. I general theory. *The Journal of Chemical Physics*, 7, 1103–1112. DOI: 10.1063/1.1750380

[25] Wang, J.W., Stevens, L.A., Drage, T.C. Wood, J. (2012). Preparation and CO_2 adsorption of amine modified Mg-Al LDH via exfoliation route. *Chemical Engineering Science*, 68, 424–431. DOI: 10.1016/j.ces.2011.09.052

[26] Rao, N., Wang, M., Shang, Z.M., Hou, Y.W., Fan, G.Z., Li, J.F. (2018). CO_2 adsorption by aminefunctionalized MCM-41: a comparison between impregnation and grafting modification methods. *Energy & Fuel*, 32, 670–677. DOI: 10.1021/acs.energyfuels.7b02906

[27] Liu, F.L., Chen, S.X., Gao, Y.T. (2017). Synthesis of porous polymer based solid amine adsorbent: effect of pore size and amine loading on CO_2 adsorption. *Journal of Colloid and Interface Science,* 506, 236–244. DOI: 10.1016/j.jcis.2017.07.049

[28] Vargas, A.M.M., Cazetta, A.L., Kunita, M.H., Silva, T.L., Almeida, V.C. (2011). Adsorption of methylene blue on activated carbon produced from flamboyant pods (Delonix regia): study of adsorption isotherms and kinetic models. *Chemical Engineering Journal*, 168, 722–730. DOI: 10.1016/j.cej.2011.01.067

[29] Liu, Y.M., Yu, X.J. (2018). Carbon dioxide adsorption properties and adsorption/desorption kinetics of amine-functionalized KIT-6. *Applied Energy*, 211, 1080–1088. DOI: 10.1016/j.apenergy.2017.12.016

[30] Volker, P., John, M., Yeon, S.H., Yury, G. (2011). Effect of pore size on carbon dioxide sorption by carbide derived carbon. *Energy & Environmental Science*, 4(8), 3059-3066. DOI: 10.1039/C1EE01176F

[31] Ana, Y.A., Víctor, M.T., Marcos, J.E.S., Ilich, A.I., Elí, S.G. (2024). Chemically Modified HKUST-1(Cu) for Gas Adsorption and Separation: Mixed-Metal and Hierarchical Porosity. *ACS Applied Materials & Interfaces*, 16(14), 65581-65591. DOI: 10.1021/acsami.4c15059

[32] Sana, Z., Sheraz, M., Muhammad, K., Natasha, S., Yan, C.L., Cumali, C., Nida, A., Asif, A., Hui, F.W., Shohreh, A., Changchun, W. (2026). Advances in mesoporous nanomaterials for photocatalytic degradation of pollutants: fundamentals, material classifications, challenges and future prospects. *Coordination Chemistry Reviews*, 549(1), 217239. DOI: 10.1016/j.ccr.2025.217239

[33] Hamid, Z., Bosirul, H., Mahmoud, A.A., Ahmed, F.S., Omar, Y.A., Mansur, A., Abdullah, M.A., Abdullah, J.A., Mahmoud, M.A. (2025). Recent advances and challenges in solid sorbents for CO_2 capture. *Carbon Capture Science & Technology*, 15, 100386. DOI: 10.1016/j.ccst.2025.100386

[34] Enhui, J., Yan, Y., Yongsheng, Y. (2025). Copper Active Sites in Metal-Organic Frameworks Advance CO_2 Adsorption and Photocatalytic Conversion. *Catalysts*, 15(9), 856. DOI: 10.3390/catal15090856

[35] Nimibofa, A., Augustus, N.E., Donbebe, W. (2017). Modelling and Interpretation of Adsorption Isotherms. *Journal of Chemistry*, 2017(1), 1-11. DOI: 10.1155/2017/3039817

[36] Despina, A.G., Athanasia, K.T., Ioannis, A.K., George, Z.K. (2025). The adsorption-desorption-regeneration pathway to a circular economy: The role of waste-derived adsorbents on chromium removal. *Separation and Purification Technology*, 368, 132996. DOI: 10.1016/j.seppur.2025.132996

[37] Abubakr, M.E., Ismat, H.A., Eid, I.B., Babiker, K.A. (2021). Evaluation of the Adsorption Efficiency on the Removal of Lead(II) Ions from Aqueous Solutions Using Azadirachta indica Leaves as an Adsorbent. *Processes*, 9(3), 559. DOI: 10.3390/pr9030559

[38] Woranart, J., Htet, M.T., Naphat, K., Kanita, C., Sorayot, C., Sira, S., Nikom, K., Poomiwat, P. (2024). Adsorption capability and regenerability of carbon slit micropores for CO_2 capture. *International Journal of Thermofluids*, 23, 100781. DOI: 10.1016/j.ijft.2024.100781

[39] Raganati, F., Alfe, M., Gargiulo, V., Chirone, R., Ammendola, P. (2018). Isotherms and thermodynamics of CO_2 adsorption on a novel carbon-magnetite composite sorbent. *Chemical Engineering Research and Design,* 134, 540–552. DOI: 10.1016/j.cherd.2018.04.037.